IX CONGRESSO BRASILEIRO DE ENGENHARIA E CIÊNCIAS TÉRMICAS
9th BRAZILIAN CONGRESS OF THERMAL ENGINEERING AND SCIENCES

Paper CIT02-0143

FLOW STRUCTURE IN THE HORIZONTAL SLUG FLOW

Eugênio Spanó Rosa
Universidade Estadual de Campinas – Faculdade de Engenharia Mecânica – Departamento de Energia
Rua Mendeleiev, s/n - Cidade Universitária "Zeferino Vaz" - Barão Geraldo - Caixa Postal 6122 - CEP: 13.083-970 - Campinas - SP
erosa@fem.unicamp.br

Abstract: *Successions of long gas bubbles and liquid slugs form the so-called slug pattern in a gas-liquid flow. A unit cell encompasses one gas bubble and one liquid slug characterizes this alternating gas and liquid flow. The kinematic and dynamic flow mechanisms responsible for the interaction between the successive unit cells are still an open question. Inside this context, this work addresses specifically to the bubble velocity, the bubble to slug interactions and the entrance mechanisms. Within an experimental framework the spatial evolution of each unit cell structure is individualized during the acquisition period. The experimental apparatus consisted of a 23.4 m long transparent Plexiglas pipe, 26mm ID, which means a total relative length of 900 free diameters. The air and water were mixed at the inlet of the test section and discharged into a collecting tank open to the atmosphere. The instantaneous measurements of the flow structure were made with double-wire conductive probes. The probes were installed in four measuring stations; each station had two probes slightly apart. The measuring stations were located at 127D, 273D, 506D e 777D from the mixer. The experimental database is further processed to give rise to histograms and correlations among flow variables*

Key Words: *slug flow, bubble velocity, drift velocity, horizontal, two-phase flow*

1. Introduction

Still today the so-called "unit cell" is the most used mechanistic representation of the gas-liquid slug flow. The concept, originally proposed by Dukler and Hubbard (1975), divides the flow in two structures. One is the liquid slug, which carries primarily liquid and some dispersed gas, in a typical dispersed bubbly flow pattern; the other is formed by an elongated gas bubble flowing over a liquid film. The structures occur successively in the pipe as the mixture flows and compose the unit cell, Fig. 1.

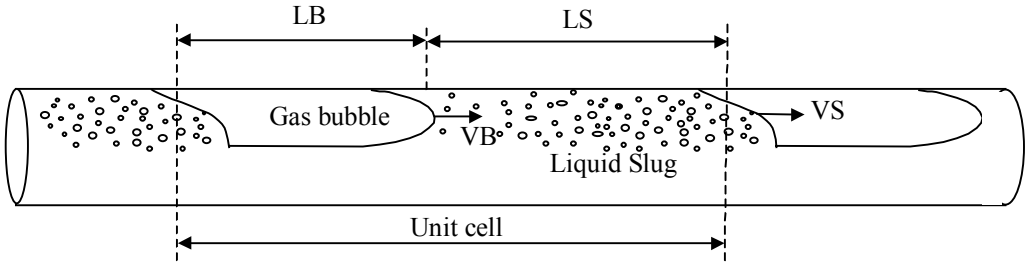

Fig. 1 - The unit cell and the mechanistic representation of slug flows.

To model the flow according this concept, one generally uses the one-dimensional time averaged mass and momentum conservation equations, complemented by constitutive relations. The conservation equations are written for inertial control volumes, one fixed and the other displacing at the velocity of the unit cell. The velocity of the unit cell is assumed to be unique, which requires the mixture flowing as a succession of identical unit cells traveling at constant velocity. Using the approach outlined it is possible to predict the averaged length of the structures, the pressure drop, the liquid hold-up and the averaged heat transfer coefficient, among other physical parameters of interest. This was, in some way, what Bendiksen (1984), Barnea and Brauner (1985), Dukler et al. (1985), Andreussi and Bendiksen (1989), Barnea and Taitel (1993) did.

Slug flow models based on the unit cell concept are relatively easy to implement. They give reliable results of average pressure and flow rates and its use is wide spread in flow simulators. The correctness of the predictions, as usual, will reflect the simplifications and the proper use of the constitutive equations that provide the closure. One major shortcoming is intrinsic to the above mentioned assumption, i.e., that *identical cells travels at constant velocity;* other refers to the constitutive equations, usually revealed by the analysis of experimental data obtained with *fully developed slug flows*. The first assumption does not attend the main characteristic of the slug flow pattern: the intermittence and irregularity. The second assumption does not consider the frequency and sizes at the section where the slugs are formed (entrance mechanism) and their evolution by coalescence (overtaking mechanism) but assume the gas-liquid structures evolving to a stationary unit size and frequency.

A better representation of the flow would result if the information on the non-uniformity of length and velocity present on a train of elongated bubbles and liquid slugs were considered. Likewise, the results would be more precise if the model could take into account the changes that the unit cells undergo as they advance in the pipe. These changes result from the interactions between successive cells, which are particularly intense up to some distance down-stream the mixer but still remains at locations far from it due to the continuous expansion of the gas. Thus, rigorously, it is not expected to achieve a space and time periodic behavior in this flow, which could be referred as a fully developed slug flow.

The kinematic and dynamical behavior of the slug flow has been experimentally investigated using statistical analysis. The histograms of the sizes and velocities downstream of the mixer arise in the work of Nydal et al. (1991) and Grenier (1997). These authors performed experiments with air/water flows in horizontal pipelines with 53 mm and 90 mm ID, respectively. Their test sections were at 312 and 1698 relative diameters long, in this order. More recently, Rosa et al. (2001 a-b) presents data on the evolution air-water slug flows in a 26 mm ID horizontal pipeline that is 900 relative diameters long. It complements the previous works in the sense that discloses experimental data taken by eight probes installed in four measuring stations located at different distances from the air-water mixer, every station having a pair of probes mounted 50 mm apart. Moreover, it reveals data on the evolution of the structures that form the unit cells as they flow along the pipe. The results include the statistical analysis and respective comparisons of the velocity and length of the elongated bubble and the aerated slug, the frequency of the unit cell and the coalescence rate. The present work further extend the previous analysis in Rosa et al. (2001 a-b) investigating experimentally the bubble velocity, the interactions between consecutive bubbles and the role of the entrance mechanism on the formation and evolution of the slug structures.

2. Experimental set up

A sketch of the experimental set-up appears in Figure 2. It includes a horizontal pipeline, storage and receiving tanks mixers, control valves, pumps, compressors and instrumentation. The test section is a 26 mm ID straight transparent Plexiglas pipeline 900 pipe diameters long, i.e., 23.4 m. The working fluids were ordinary tap water and compressed air. High capacity compressors and a centrifugal pump supply the air and the water to the mixer installed at the entrance of the test section. Two different mixers have been used in order to detect the influence of the mixing process on the formation and evolution of the slug flow. The first mixer was made of two concentric tubes, here after called by concentric stream mixer, CSM. The inner tube delivers the air through a small orifice while the water flows trough the annular space. The second mixer was made of a single tube with a Plexiglas sheet dividing its cross section in two separated channels, also called by parallel stream mixer, PSM. Two parallel streams of water and air are formed inside the mixer and put together at the outlet. The use of CSM or PSM is to observe the differences on the flow structures at the slug formation processes and how these structures evolve along the pipe. At the other end of the test section the mixture is discharged, without restraint, into a receiving tank open to the atmosphere (in average, 0.94 bar and 25^{o}C). From the receiving tank the water is transferred to the main tank, so that the total volume contained by the system adds-up to 3 m^{3}, ensuring a fairly constant water temperature during the experiment.

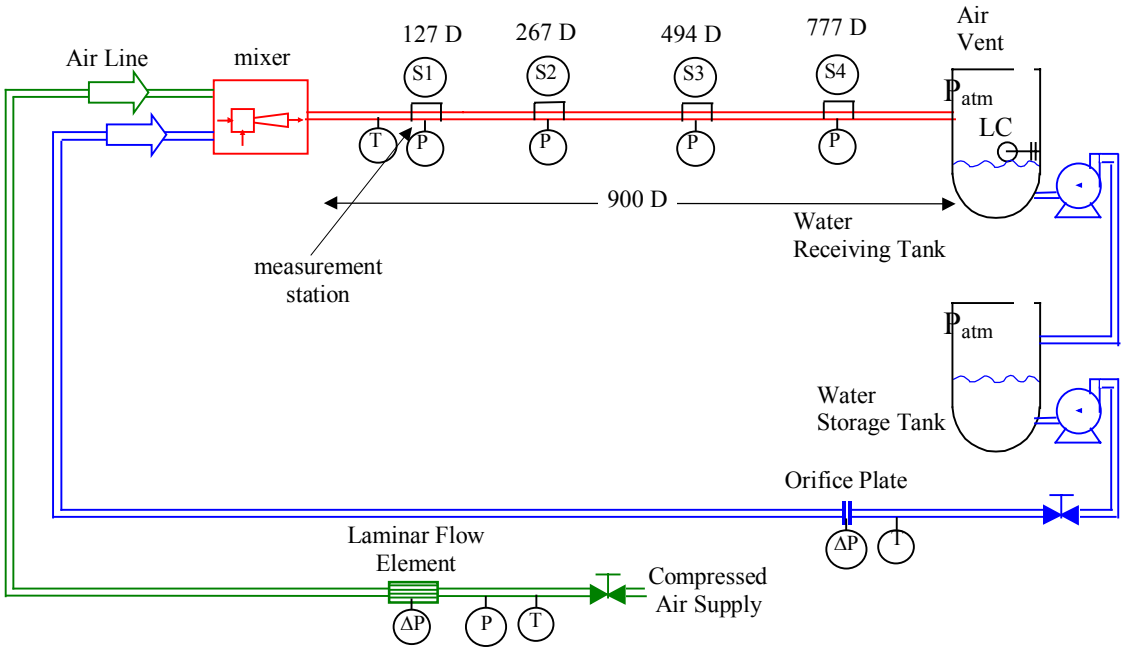

Figure 2. Schematics of the experimental set up.

The water flow-rate was measured by a set of three orifice plates that were calibrated at 1½% of monitored uncertainty. To measure the air flow-rate one used two Merian© laminar flow elements with reported an uncertainty of 1%. The range of air superficial velocities varied between 0.4 Sm/s to 1.7 Sm/s. The water superficial velocities ranged from 0.25 m/s to 1.35 m/s. The letter S in front of the unit specify the local atmospheric condition (0.947 bar @ 21°C); otherwise it refers to the *in situ* conditions.

Besides the flow rate instrumentation and specific probes measuring the flow in the test section, there were various temperature and pressure transducers monitoring the operation of the experimental set-up and transmitting the signals to a data acquisition system.

In every station is installed a pair of double-wire probes, 50 mm apart, and a pressure transducer, which measures the instantaneous the liquid film thickness and pressure necessary to correct the air flow-rate. To identify and measure the structures of the slug flow such as the propagation velocity, the frequency, the length and the coalescence rate, as they evolve along the pipeline were used double–wire conductive probes and signal conditioning circuits. These measurements were performed, simultaneously, in four measuring stations distributed along the pipeline, S1 to S4 in Fig. 2.

Typical signals, taken simultaneously by the twin probes of a measuring station appear shifted in time in Fig. 3. The liquid film flows bellow or, sometimes, surrounding the elongated bubble, and creates the low-level signal. The liquid slug produces the high level signal. This time-based signal gives a rough discrimination of the structures that compose the unit cell.

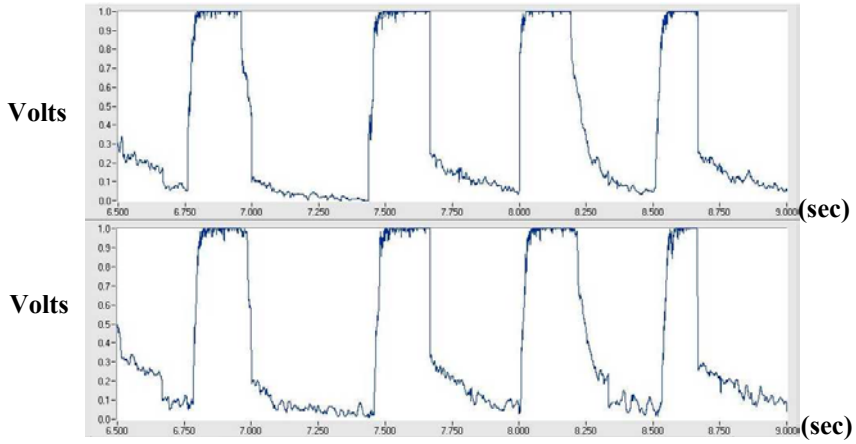

Figure 3. The time signals delivered by the double-wire probes mounted in a measuring station, amplitude (V) versus time (s), grabbed from the computer screen.

The probes driving circuit, the sampling frequency and further treatment of the raw data are described in Rosa et al. (2001 a-b) and will not be reproduced here. Even tough is necessary to say that the voltage signal is transformed in a sequence of square waves with minimum and maximum of 0 and 1 by applying a cut-off voltage. Voltages values above the cut-off value became (1) otherwise (0) and are associated with the occurrence of the liquid slug or the elongated bubble, respectively. Figure 4 shows a representative sample of the square wave signals, obtained after applying a proper threshold level to the original voltage signals.

The resistive probes measure the time of liquid and gas events inside the pipe from an Eulerian frame of reference. Taking for reference Fig. 4, the wave in the upper part of the plot is referred to the front sensor, in the lower part it is referred to the rear signal. The i^{th} liquid slug trailed by the ith-elongated bubble composes the i^{th} unit cell. B(i) and S(i) specifies the time of occurrence of the bubble front and the slug front, respectively. The subscript $_{(F)}$ and $_{(R)}$ refers to the front or rear probe, convention established in regard the flow direction. The values of the unit period, and the velocities of the bubble and slug fronts are determined using the time records of the twin probes. The period of the i^{th} unit cell is evaluated as:

$$T(i) = S_F(i) - S_F(i-1) \tag{1}$$

The bubble and slug front velocities, VB(i) and VS(i), are estimated as the ratio of the probe spacing (s = 50mm) and the time delay between the front and rear sensor events:

$$VS(i) = \frac{s}{[S_R(i) - S_F(i)]}, \quad VB(i) = \frac{s}{[B_R(i) - B_F(i)]}. \tag{2}$$

While the VS and VB are considered to be the instantaneous velocities, the same does not apply to the length estimates. The difficulty arises because for length determination is necessary velocity measurements following the bubble or the slug, i.e., in a Lagrangian frame of reference. The length rate of change with time is prescribed by the velocity difference between the fronts,

$$\frac{d}{dt}LB(i) = VB(i+1) - VS(i) \quad \text{and} \quad \frac{d}{dt}LS(i) = VS(i) - VB(i)\ . \tag{3}$$

The recorded velocities correspond to the i^{th} bubble front and bubble tail (or slug front) but they are delayed in time owing to the length of the bubble, which is typically several pipe diameters long. Therefore instantaneous front and tail velocities are never known at the same instant because the probes are stationary. At the pipe entrance the slugs are developing, their lengths are growing and Eq. (3) must be enforced. Further downstream the sizes of the units have slow changes with time, the length may be estimated by:

$$LB(i) = VB(i)\cdot\left[S_F(i) - B_F(i)\right] \quad \text{and} \quad LS(i) = VS(i)\cdot\left[B_F(i) - S_F(i-1)\right], \tag{4}$$

implying that the front and the tail of the bubble moves with the same velocity VB. The same applies for the slug, the front and the tail of the slug moves with the same velocity VS.

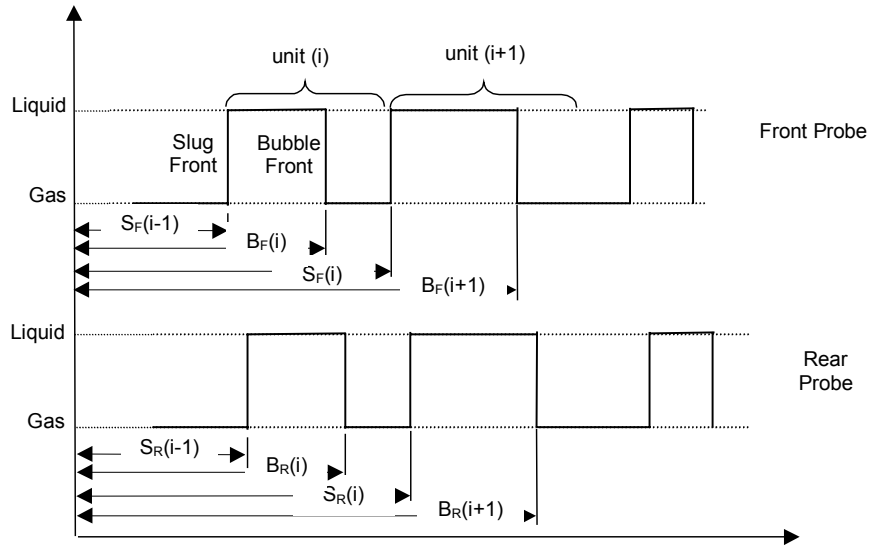

Fig. 4 A pair of square-wave signals identifying the structures of the slug and bubble fronts.

The outcome of post-processing the experimental data is an array representing the velocity, length and period of every elongated bubble and liquid slug that passed by the sensors. It is then further processed statistically, giving rise to average values, standard deviations, histograms and correlation coefficients. From here on, for sake of conciseness, the average value of a generic discrete variable x will appear as <x>, the standard deviation as Sx and the correlation coefficient Rxy. They are evaluated as:

$$\langle x\rangle = \frac{1}{N}\sum_{i=1}^{N} x_i \qquad S_x = \sqrt{\frac{1}{N-1}\sum_{i=1}^{N}\left[\langle x\rangle - x_i\right]^2} \qquad R_{xy} = \frac{\frac{1}{N-1}\sum_{i=1}^{N}\left[\langle x\rangle - x_i\right]\cdot\left[\langle y\rangle - y_i\right]}{S_x \cdot S_y} \tag{5}$$

3. Experimental results

The structures of slug flows have been identified at the four measuring stations for various flow rates. For each mixer type were conducted nine experimental runs at the same pair of air and water superficial velocities, as identified in Table 1. The water and the air superficial velocities spanned from 0.25 m/s to 1.33 m/s, and 0.33 Sm/s to 1.67 Sm/s, respectively. The number of unit cells indicates the size of the sample in terms of valid unit cells, which passed through the sensors during the acquisition period. For convenience is also shown in Table 1, the mixture pipe Reynolds number, the Froude number and Eotvos number are defined as:

$$Re = \frac{J\cdot d}{\nu_L}, \qquad Fr = \frac{J}{\sqrt{gd}}, \qquad Eo = \frac{\rho_L g d^2}{\sigma}, \qquad \text{where} \quad J = JL + JG, \tag{6}$$

and J is the mixture superficial velocity, σ is the air-water surface tension, ν and ρ represent the water kinematic viscosity and density, respectively and d is the pipe diameter. A photographic record of the bubble tail and nose is shown in Fig. 5 for runs #1, #2, #3, #5, #6 and #7. The photographs come from frozen frames of a black and white high-speed digital movie recorded at 494 diameters downstream of the concentric mixer, station S3. The frames picture the measuring station and are approximately four pipe diameters long. To help identify the interface a hand drawn line is superposed on the actual picture. It enhances the contours of the bubble tail and nose shapes. As a further information,

all frames show two straight and vertical bright lines. They are the twin parallel gold wires stretched across the pipe section and 50 mm apart from each other. For run #1, is observed a well-defined bubble nose with a stable shape attached to the pipe top wall. An increase on the gas flow rate, as occurs from run #1 to #3, causes the bubble nose to bend toward the pipe center in an irregular shape with a not stable interface. The bubble tail has always an angle greater than ninety degrees with respect to the base liquid film. For the present runs, the bubble tail has dispersed bubbles for air to water flow ratio greater than unit. Runs #1 and #5 have negligible air content within the liquid slug. The length of the aerated volume on the liquid slug is within 1 to 4 pipe diameters, with the exception of #8 and #9.

Table 1 – Superficial velocities, number of unit cells, acquisition period, Reynolds, Froude and Eotvos numbers for each run.

Run #	JG (Sm/s)	JL (m/s)	Number of unit cells	Acquisition Period (s)	Re (x 10^4)	Fr	Eo
1	0.33	0.67	350	600	2.7	2.0	95
2	0.33	1.33	360	600	1.3	3.3	95
3	0.33	1.67	320	600	5.0	4.0	95
4	0.50	0.50	470	360	2.6	2.0	95
5	0.67	0.67	700	360	3.3	2.7	95
6	0.67	1.33	550	360	5.0	4.0	95
7	0.67	1.67	500	360	6.0	4.7	95
8	1.33	0.67	1600	240	5.0	4.0	95
9	1.33	1.33	1400	240	6.5	5.3	95

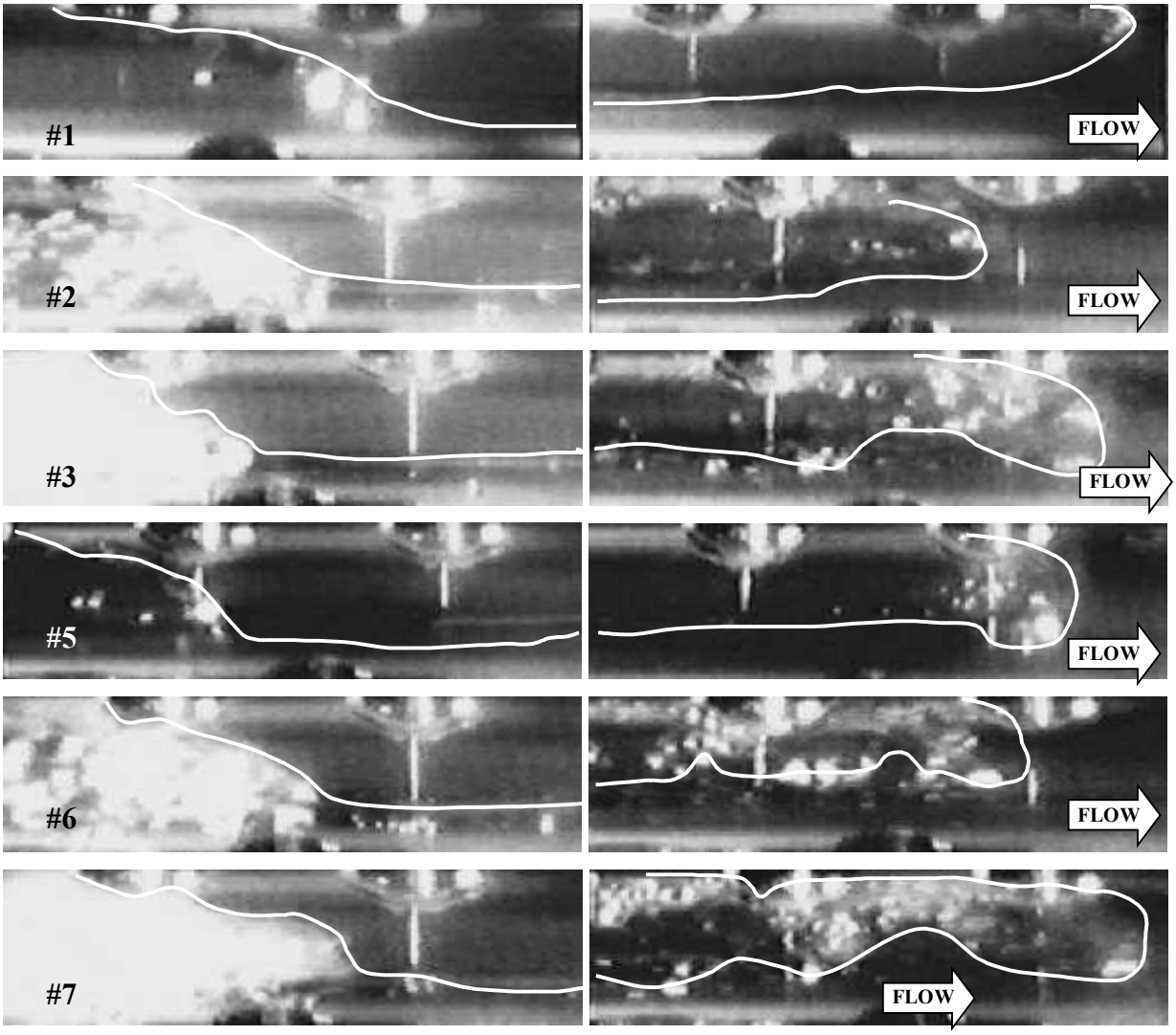

Fig. 5 – Photographs of the slug front and bubble tail for runs #1, #2, #3, #5, #6 and #7.

3.1 The velocity of the elongated bubble

Most of the transported gas is carried within the elongated bubble. An accurate prediction of the gas flow rate needs detailed knowledge on the bubble shape and its velocity. The present section deals with the nose velocity of the elongated bubble in a presence of a train of slug units.

Several theoretical and experimental approaches regarding this matter were performed in the past. Based on experiments with a isolated bubble Nicklin et al (1962) proposed a linear "drift-flux like" relationship to determine the bubble nose velocity, VB,

$$VB = C_0 \cdot J + V_\infty , \tag{7}$$

where the constants C_0 and V_∞ are associated, in order, to the phase's distribution and to the bubble drift velocity in a fluid at rest. The constants C_0 and V_∞ are in fact dependent on several parameters such as pipe diameter, pipe inclination angle, mixture velocity, surface tension and liquid viscosity among others Fabre and Liné (1992). It is not straightforward to extend the behavior of a single bubble to a train of bubbles. Its motion is influenced by the dynamic interactions caused by the neighboring unit cells. Nevertheless, the insight gained by the theoretical and experimental analysis of single bubble experiments sheds light on the experimental analysis of a train of bubbles. The idea behind the relationship proposed by Nicklin is put forward on train of bubbles as the bubble translation velocity is composed by superposition of the mixture velocity and the drift velocity. According to Bendiksen (1984), the coefficients C_0 and V_∞ for horizontal flows are usually chosen as:

$$\begin{aligned} &C_0 = 1.0 \text{ and } \quad V_\infty = 0.54 \quad \text{if} \quad Fr < 3.5 \\ &C_0 = 1.2 \text{ and } \quad V_\infty = 0.00 \quad \text{if} \quad Fr \geq 3.5 \end{aligned} \tag{8}$$

For regimes where the $Fr < 3.5$ there exists a gravity-induced drift resulting from the elevation difference in the bubble nose, Benjamin and Broke (1968). For Froude values greater than 3.5 the inertia force overcome the gravity force and the drift velocity on the horizontal slug flow is zero. A direct comparison between the experimental determined coefficients and the accepted Bendiksen values, Eq. (8) is drawn. The averaged bubble velocity is presented against the mixture velocity in Fig. 6.

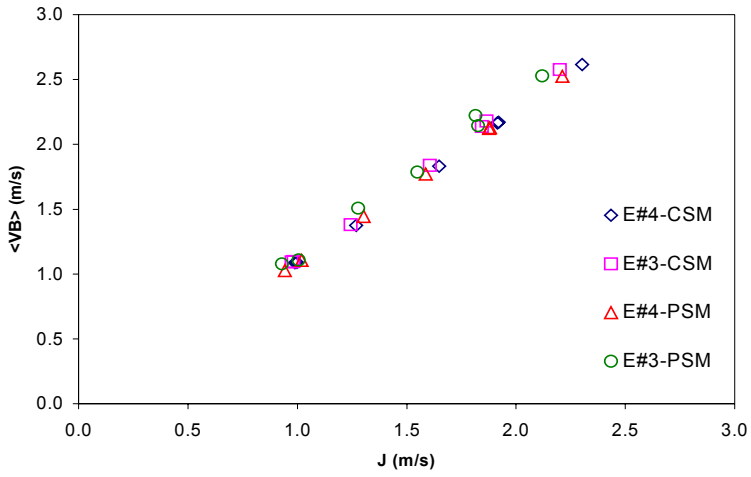

Fig. 6 – Averaged bubble nose velocity against mixture velocity. Data for measuring stations S3 and S4 for CSM and PSM mixers.

The selected data come from the experiments using the concentric and parallel stream mixers. The sample size of each run is in Table 1. The presented bubble nose velocity is only for stations S3 and S4 where the entrance effects are fading away. Stations S3 and S4 reproduce the closest conditions that prevailed to get the constants of Eq. (8). The experimental values of the constants C_0 and V_∞ result of a least square fit displayed on Table 2. The data belonging to each station fits remarkably well by the linear relation of Eq. (7) exhibiting a R squared value of 0.99 or greater. It is observed a mild decrease of C_0 considering the distance from the mixer while V_∞ is nearly constant through out the stations S3 and S4. The influence of the formation mechanism imparted by the use of different mixers is not observed on stations S3 and S4. In fact, considering the same stations for comparison basis, the C_0 and V_∞ values agree within 3% for both cases. Furthermore the C_0 and V_∞ values do not show any dependence on the Froude number, as suggested by Bendkisen. Considering the flow regimes where $Fr > 3.5$, the C_0 values found experimentally agrees well with the published data although, the drift velocity was found not zero but with negatives in all cases.

The sample size, the data repeatability and linearity, and also the flow measurement accuracy and the horizontal alignment of the pipeline rack, are favorable indicators of the data consistency. Based on the experimental evidence it is argued the possibility of the existence of negative drift. In fact the absence of gravitational force along the horizontal direction does not ensure a positive nor zero drift while the negative slope is the necessary condition to happen negative drift. The negative drift means that in average the gas is slower than the liquid but it depends of the space-wise and time-wise distribution of the liquid and gas phases. It cannot be misunderstood as local phenomena. It is possible that the tip of the nose may travel faster than the liquid ahead of it while in term of averaged value results in a negative drift. An evidence of it is the pointing direction of the bubble that depends on the local liquid velocity field ahead of it. One may argue that negative drift may cause the bubble tip be aligned against the flow direction. But, this is not observed for a -2^o inclination pipe with the bubble nozzle still aligned with the flow direction, Bendiksen (1984).

Table 2. The C_0 and V_∞ constants resultant from a least square fit of the experimental data.

	Station	C_0	V_∞ (m/s)	R^2
Concentric	S3	1.22	-0.11	0.999
Stream Mixer	S4	1.17	-0.09	0.999
Parallel	S3	1.25	-0.11	0.995
Stream Mixer	S4	1.18	-0.10	0.999

The existence of negative drift has also implications on the coupling of dynamic forces between the bubble and the liquid slug. This subject is discussed on the next section.

3.2 Liquid slug to neighboring bubble interactions

The interactions between the liquid slug and the neighboring bubbles are responsible to the intermittent behavior. They cause changes in the speed, which result in changes on the lengths that may end up in bubble coalescence if two consecutive bubbles touch each other. When two bubbles merge to a single one the size of the bubble increase, the volume of liquid slug between then is displaced to the neighboring slug and the unit period changes. This phenomenon of bubble coalescence is known by bubble overtaking. The interactions between the gas and liquid structures are higher at the flow entrance exhibiting a high coalescence rate Rosa et al.(2001 a-b). Increasing the distance from the mixer, the coalescence rate decreases exponentially, the average quantities such as sizes and velocities change slowly but the intermittent behavior still exists. Duckler et al. (1985) uses this slow change properties region to establish a minimum stable slug length where the influence on the trailing bubble is negligible. They argue about the minimum slug length necessary to establish a fully developed velocity profile ahead of the trailing bubble. Prior to this, Moissis and Grifth (1962) proposed a kinematic dependence on the trailing bubble velocity with the liquid slug length ahead of it. The original relationship was developed based on the interactions of two isolated bubbles flowing in ascendant vertical direction. They found that the trailing bubble velocity is a function of the separation distance between bubbles, and fitted the experimental data using a exponential decay law with the distance:

$$\frac{VB_T}{VB_L} = 1 + 8\exp\left(-1.06 \cdot \frac{LS}{D}\right), \tag{9}$$

where the subscripts T and L stands for trailing and leading bubble velocity. Barnea and Taitel (1993) used a similar relation with different coefficients for the horizontal case. More recently, Fagundes (1999) further improved the kinematic relation for horizontal flow but still based his results on two bubbles interaction.

The present work investigates experimentally this general kinematic law in a presence of a train of bubbles. To get reliability on the lengths estimates is used the database from station S4, 777D downstream the mixer. At S4, the histograms of the bubble nose and slug front difference velocities are symmetric with mean value near zero indicating that the rhs of Eq. (3) is zero and the assumptions made in Eq. (4) holds. Three interaction mechanisms are investigated in terms of correlation coefficients, they are: a) the dependence of the bubble nose velocity on the length of the liquid slug ahead of it, b) the dependence of the logarithm of the leading bubble to the trailing bubble velocity ratio on the slug length between then and c) the dependence on the drag force on the pressure gradient across the bubble.

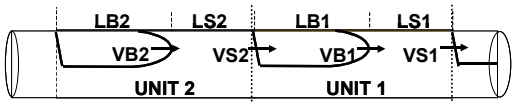

Fig 7 – Nomenclature for the neighbor unit cells

The variables employed to constitute the correlation coefficients are labeled in Fig. 7 by identifying two consecutive units in Fig. 7 and associating the indexes (1) and (2) to the leading and to the trailing units. The first two correlations follow the Moissis and Griffith kinematic law. For case (a) R(a) seeks if the faster bubbles come after the shorter slugs, and for case (b) R(b) search if the trailing bubble to the leading bubble velocity ratio depends on the slug length.

$$R_{(a)} = \frac{\frac{1}{N-1}\sum_{i=1}^{N}\left[\langle VB1\rangle - VB1_i\right]\cdot\left[\langle LS1\rangle - LS1_i\right]}{S_{VB1}\cdot S_{LS1}} \qquad R_{(b)} = \frac{\frac{1}{N-1}\sum_{i=1}^{N}\left[\left\langle Ln\left(\frac{VB2}{VB1}\right)\right\rangle - Ln\left(\frac{VB2}{VB1}\right)_i\right]\cdot\left[\langle LS2\rangle - LS2_i\right]}{S_{Ln(VB2/VB1)}\cdot S_{LS1}} \tag{10}$$

The case (c) express a force balance on the bubble comprised between two consecutive liquid slugs. Extending the use of BBO equation (Crowe et. al. 1998) the net force on the bubble is expressed by:

$$\overbrace{\rho_B LB\cdot A_B\frac{dVB}{dt}}^{M_{Air}} = \overbrace{\rho_S LB\cdot A_B\left(\frac{1}{\rho_S}\frac{dP}{dx}\right)}^{M_{Water}} - A_B\cdot\rho_S\frac{1}{2}C_D(VB-VS)^2\cdot\frac{(VB-VS)}{|(VB-VS)|} - \overbrace{\rho_S\cdot LB\cdot A_B C_{VM}\frac{D(VB-VS)}{dt}}^{M_{Water}} \tag{11}$$

bubble accel; pressure grad.; drag; virtual mass

where the net force on the bubble is equal to the pressure gradient exerted by the liquid plus the drag force due to the bubble relative motion and finally the virtual mass acceleration. The Basset force and the buoyancy force were excluded from eq. (11). Further simplifications on Eq. (11) are done considering the flow acceleration is not changing quickly and the air density is much smaller than the water density. The last two assumptions reduce Eq. (11) to a balance between the pressure gradient against the drag force. Actually the pressure on the bubble is constant but there is a normal pressure force acting on the liquid slugs ahead and from behind the bubble that causes the extra push. The pressure force arises because the slug front velocities are almost independent from the neighboring units (see RVS1xVS2 in Table 3). The liquid slugs traveling at different speeds ahead and behind the bubble build up a normal pressure difference across the bubble nose and tail. Neglecting the viscous terms, the pressure gradient term is estimated as:

$$\left(\frac{1}{\rho_L}\frac{dP}{dx}\right) \approx VS1\cdot\frac{(VS1-VS2)}{L1}. \tag{12}$$

Replacing Eq. (12) in Eq. (11) and considering the above simplifications, the force balance reduces to:

$$C_D\frac{1}{2}(VB1-VS1)^2 \approx VS1\cdot(VS1-VS2)\cdot\left(\frac{LB1}{L1}\right). \tag{13}$$

Therefore the correlation coefficient for mechanism (c) is:

$$R_{(c)} = \frac{\frac{1}{N-1}\sum_{i=1}^{N}\left[\left\langle(VB1-VS1)^2\right\rangle - (VB1-VS1)^2{}_i\right]\cdot\left[\left\langle VS1.(VS1-VS2).\frac{LB1}{L}\right\rangle - \left(VS1.(VS1-VS2).\frac{LB1}{L}\right)_i\right]}{S_{(VB1-VS1)^2}\cdot S_{VS1.(VS1-VS2).\frac{LB1}{L}}} \tag{14}$$

Scatters plot of the variables involved in mechanisms (a), (b) and (c) are shown in Fig. 8 for run #4 with data taken from station S4 using a PSM mixer. Figure 8(a) shows the bubble velocity against the liquid slug length ahead of it. Figure 8(b) has the logarithm of the leading bubble to trailing bubble velocity ratio against the slug length between them. Finally, Figure 8(c) exhibits the balance between the pressure and drag force acting on the bubble. Anticipating the correlation coefficient analysis, Fig. 8 does not reveal a bubble velocity dependence on the slug length, cases (a) and (b). On the other hand the sequence of slugs and bubble do show some definite trend for the drag and pressure force balance.

The degree of the linear relationship between the variables involved on the studied cases (a), (b) and (c) is displayed on Table 3 as the linear regression coefficients defined in Eqs. (10) and (14). The data is taken from station S4 for runs #1 to #9. The mixer type used is also displayed on the table. The R(a) reveals a weak correlation concerned with the bubble velocity and the slug length. The dependence of the trailing bubble to leading bubble velocity ratio on the slug length also resulted in a linear correlation coefficient less than 0.12 for all cases. Surprisingly, the pressure and drag force balance indeed show a good correlation coefficient, in fact it stayed $0.43 < R(c) < 0.83$ for 18 runs including both mixers types.

3.3 Entrance mechanism

It is of particular interest to investigate if the characteristic lengths and velocities of the bubble and of the liquid slug are controlled by entrance mechanisms acting during the slug formation or if the overtaking mechanisms and bubble to slug interactions define them. This task was accomplished experimentally generating slug flow by means of different entrance mechanism: buoyancy force and bubble coalescence in one type of air-water mixer and Kelvin-Helmoltz instability on the other. The two types of mixers are the concentric stream mixer, CSM, and the parallel

stream mixer, PSM. The CSM mixer issues a concentric air jet surrounded by water flowing on the annular space. The air jet is broken into small bubbles, which are quickly carried by the water stream. Owing to the buoyancy force, the bubbles migrate to the top of the pipe, coalesce, form large bubbles surrounded by liquid pistons that evolve to the known slug flow pattern. The PSM uses an internal plate to divide the pipe cross-section into two parallel channels. Along the bottom one flows the water stream and on the top flows the air stream. The mixer is about 10 pipe diameters long. After this distance the water and air streams are put together. A Kelvin Helmoltz type instability develops along the air-water interface. It forms growing waves, which block the pipe cross section, and ends up establishing the slug flow pattern.

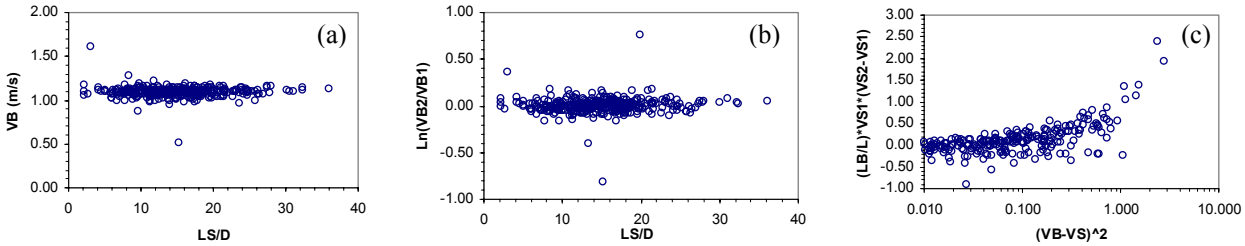

Fig. 8 – Scatter plots for slug to bubble interaction mechanism (a), (b) and (c) for taken at station S4 using PSM mixer for run #4.

Table 3 – Correlation coefficients R(a), R(b) and R(c) taken at station S4, using PSM and CSM mixers, for runs #1 to #9. The last column is the correlation coefficient for the slug velocity of two consecutive units.

Correlation Mixer Type Run	R(a) PSM	R(b) PSM	R(c) PSM	R(c) CSM	R(VS1XVS2) PSM
#1	+0.21	+0.12	+0.73	+0.68	-0.02
#2	-0.08	-0.04	+0.46	+0.58	-0.02
#3	+0.03	-0.02	+0.48	+0.58	-0.05
#4	+0.04	-0.03	+0.65	+0.71	+0.01
#5	+0.12	+0.08	+0.61	+0.68	+0.09
#6	+0.05	+0.01	+0.79	+0.77	-0.01
#7	-0.01	-0.07	+0.65	+0.83	-0.08
#8	-0.01	-0.07	+0.62	+0.53	-0.01
#9	+0.04	+0.05	+0.73	+0.65	+0.01

Experimental data for runs #2 and #6 relative to the slug and bubble instantaneous front velocities, VS and VB, are taken along the four measuring stations using the CSM and the PSM mixers. The data is further processed to give rise to histograms of VS and VB. The run#2 data histogram is shown in Fig. 9 while for run#6 is in Fig. 10.

Considering Fig. 9 at station S1, where the entrance effects are dominant, the VB and VS distributions are quite distinct from each other. The area blockage of the air injector causes the CSM mixer to produce bubbles with a higher mean velocity than the PSM mixer. Due to the occurrence of small bubbles during the slug formation, the CSM mixer generates VB and VS with a large standard deviation when compared against the PSM mixer. As the flow evolves to station S3 and S4 the changes on the population are minor, the flow becomes more ´organized´ in a sense that the VB and VS samples have smaller standard deviation. Also the similarities between the CSM and PSM samples start arising due to the similarities among the histograms. This is an indication that the entrance effects are fading away, but even at 777 D downstream the mixer small differences on the samples frequencies are still detected.

Figure 10 depicts the histograms for run#6. The overall behavior of the histograms is the same of run#2. The exception for run#6 is that the VB and VS histograms at S4 for CSM and PSM mixers are identical. This indicates that the flow entrance mechanisms have no effect at 777 D downstream the mixer. The population exhibits the same mean and standard deviation.

4. Conclusions

The mean velocity of the elongated bubble has a linear dependence with the mixture superficial velocity. The dependence with the Froude number on C_0 and V_∞ was not found. The constant C_0 agrees with the published value of 1.2 but the drift constant, V_∞ does not. In fact V_∞ was found negative while the literature report a zero value due to the absence of gravity along the flow direction. The literature results may be questionable if one observes the pictures of the unstable air-water interface at the bubble nose. It is not plausible that these structures travel along the pipe with no slip, that is, with no drag. The small difference found in V_∞ for Fr > 3.5 when compared with the recommended value, see

Eq. (8), is not significant when evaluating VB as suggested by Eq. (8). Nevertheless this difference in V_∞ pointed to a new mechanism of bubble-slug interaction. The experimental data show some correlation ($0.43 < Rc < 0.83$) on the balance between the drag and pressure forces. The velocity difference of the slug fronts from ahead and from behind the bubble causes a pressure difference that is balanced by the bubble drag force induced by its relative velocity. This mechanism establishes a link between the bubble velocity and the slug front velocity from ahead and from behind the bubble. Considering a sequence of unit cells this type of mechanism is capable to couple all the units within the pipe. On the other hand it was not observed, for the train of bubbles, any dependence of the bubble velocity with the slug length ahead of it. Finally, it was observed that the entrance effects fade away after a downstream distance from the mixer. The resulting distributions of VB and VS are found the same despite of being generated by different entrance mechanisms.

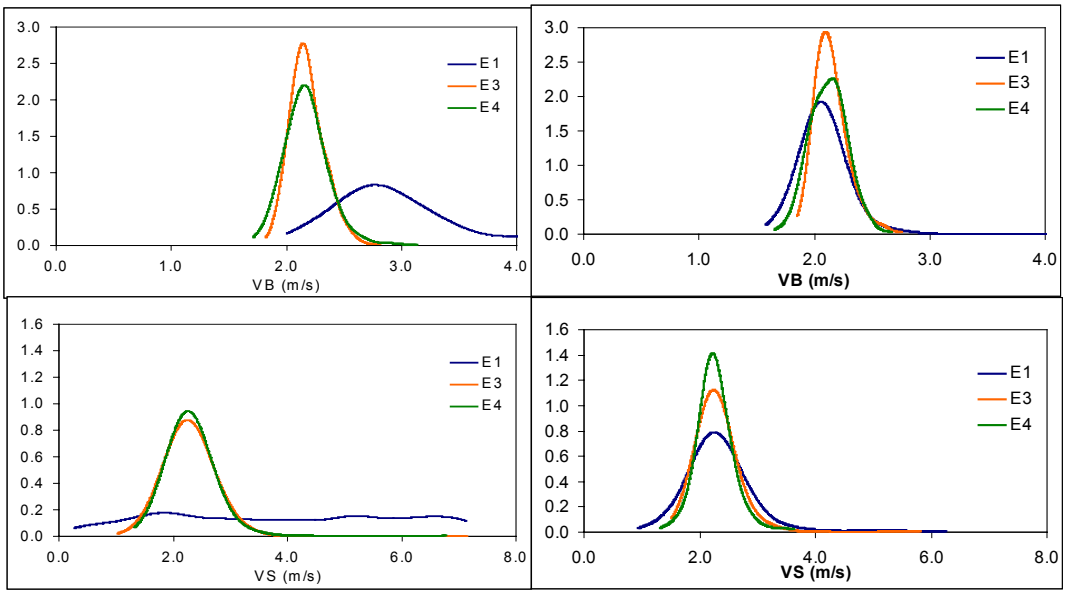

Fig. 9 - VB and VS histograms for run#2 generated by CSM mixer (left column) and PSM mixer (right column).

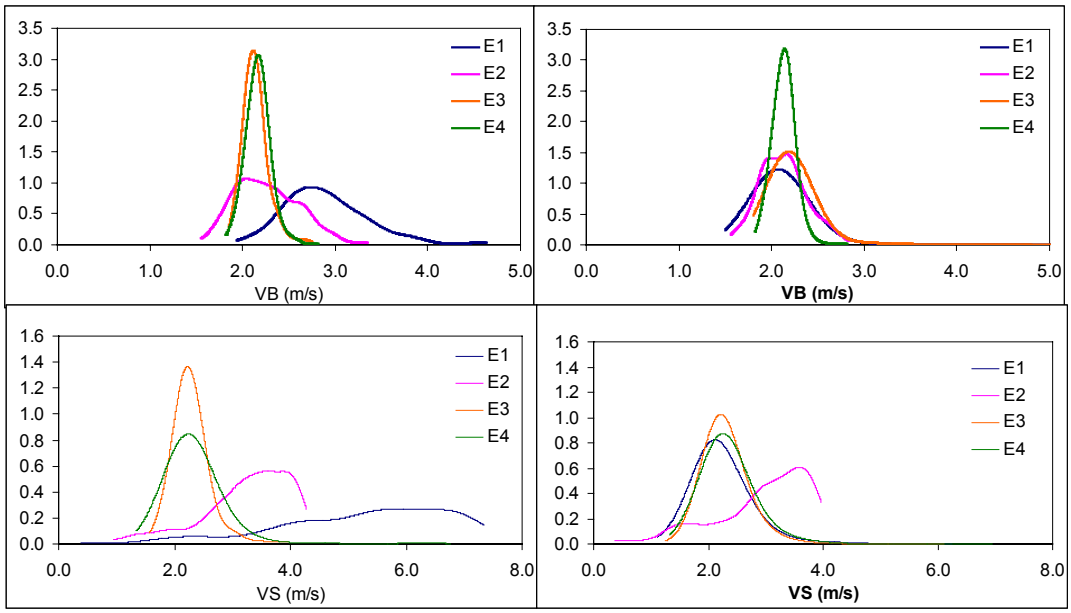

Fig. 10 - VB and VS histograms for run#6 generated by CSM mixer (left column) and PSM mixer (right column).

5. Acknowledgments

This work was funded by the FINEP-CTPETRO projects n. 65.2000.0043.00 and n. 2101034100 and Petrobras. The author is grateful to Dr. Fagundes Netto from Petrobras, for the useful suggestions and constant encouragement.

6. References

Andreussi, P. and Bendiksen, K., 1989, "An investigation of void fraction in liquid slugs for horizontal and inclined gas-liquid pipe flow", Int. J. Multiphase Flow, vol15, pp. 937-946.

Benjamin, T. Brooke, 1968, "Gravity Currents and Related Phenomena", J. Fluid Mech., vol.31, part 2, pp. 209-248.

Barnea, D. and Brauner, N., 1985, "Holdup of the liquid flow in two-phase intermittent flow", Int. J. Multiphase Flow, vol 11, pp. 43-49.

Barnea, D. and Taitel, Y, 1993, "A model for length distribution in gas-liquid flow", Int. J. Multiphase Flow, vol 19, pp. 829-837.

Bendiksen, K.H., 1984, "An Experimental Investigation of the Motion of Long Bubbles in Inclined Tubes", Int. J. Multiphase Flow, vol 10, n. 4, pp. 467-483.

Crowe, C., Sommerfeld and M. and Tsuji, Y., 1998, "Multiphase Flows with Droplets and Particles", CRC Press, 471 p.

Dukler, E. and Hubbard, M.G., 1975, "A model for gas-liquid slug flow in horizontal and near horizontal tubes", Ind. Eng. Chem. Fundam., vol 14, n.4, pp.377-347.

Dukler, E., Maron, D.M. and Brauner, N., 1985, "A physical model for predicting the minimum stable slug length". Chem. Eng. Sci., 40: 1379-86.

Fabre, J. and Liné, A., 1992, "Modeling of two-phase slug flow", Annual Review of Fluid Mech., 24:21-46.

Fagundes Netto, J.R, 1999, Dynamique de Poches de Gaz Isoléesen écoulement Permanent et Non-permanent Horizontal", Ph.D. thesis, Institut National Polytechnique de Toulouse, France.

Grenier, P., 1997, "Evolution des longuers de bouchons écoulement intermittent horizontal", Ph.D thesis, Institut National Polytechnique de Toulouse, France.

Moissis, R. and Griffith, P., 1962, "Entrance effects in a two-phase slug flow", J. Heat Transfer, pp. 29-39.

Nicklin, D.J., Wilkes, J.º and Davidson, J.F., 1962, "Two-phase Flow in Vertical Tubs", Trans. Inst. Chem. Engng, vol.40, pp61-68.

Nydal, O.J., Pintus, S. and Andreussi, P., 1992, "Statistical characterization of slug flow in horizontal pipes", Int. J. Multiphase Flow, 18,3,pp. 439-453.

Rosa[(a)] , E.S.; Morales, E.R; Melo, A.I., Freire, R. and França, F.A., 2001, " The Evolution of Horizontal Slug Flow", XVI Congresso Brasileiro Eng. Mecânica, COBEM, Uberlândia, 26 a 30 de Nov., pp. 1 a10, CD ROM.

Rosa[(b)] , E.S., Morales, E.R., Melo, A.I.; Freire, R.C. and França, F.A. ; "The Slug Flow Evolution in a Horizontal Pipeline", Canadian International Petroleum Conference, 2001 Calgary, Alberta – Canada, June 12-14, paper 2001-176, 14 pages.